



Contents lists available at ScienceDirect

# Spectrochimica Acta Part A: Molecular and Biomolecular Spectroscopy

journal homepage: [www.elsevier.com/locate/saa](http://www.elsevier.com/locate/saa)

## Solvatochromism of symmetrical 2,6-distyrylpyridines. An experimental and theoretical study



Jelena M. Marković<sup>a</sup>, Nemanja P. Trišović<sup>a,\*</sup>, Dragosav Mutavdžić<sup>b</sup>, Ksenija Radotić<sup>b</sup>, Ivan O. Juranić<sup>c</sup>, Branko J. Drakulić<sup>c</sup>, Aleksandar D. Marinković<sup>a</sup>

<sup>a</sup> Faculty of Technology and Metallurgy, University of Belgrade, Karnegijeva 4, 11000 Belgrade, Serbia

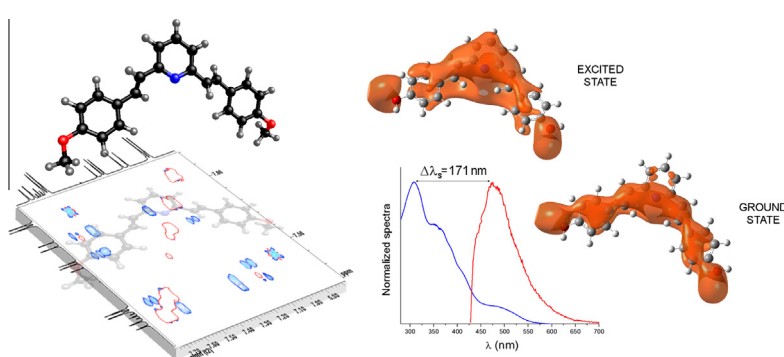
<sup>b</sup> Institute for Multidisciplinary Research, University of Belgrade, Kneza Višeslava 1, 11000 Beograd, Serbia

<sup>c</sup> Department of Chemistry, Institute of Chemistry, Technology and Metallurgy, University of Belgrade, Njegoševa 12, 11000 Belgrade, Serbia

### HIGHLIGHTS

- Synthesis and spectroscopic properties of symmetrical 2,6-distyrylpyridine derivatives are described.
- Population of conformers in solution was estimated by NAMFIS analysis, from NMR data.
- Solvent effects on the UV–Vis spectra are evaluated by the Kamlet–Taft and Catalán LSER models.
- The decomposition of the emission spectra is performed using MCR analysis.

### GRAPHICAL ABSTRACT



### ARTICLE INFO

#### Article history:

Received 16 May 2014

Received in revised form 11 July 2014

Accepted 15 July 2014

Available online 24 July 2014

#### Keywords:

UV–Vis spectroscopy

Fluorescence spectroscopy

Conformational preferences

### ABSTRACT

Seven symmetrical 2,6-distyrylpyridines, phenyl-substituted with hydrogen-bond donors, hydrogen-bond acceptors, halogens and hydrophobic moieties were synthesized and their spectroscopic characterization was done. Solvent effects on the absorption and fluorescence spectra were analyzed and quantified using the Kamlet–Taft and Catalán approach. The obtained results were rationalized by comparison of electrostatic potentials of the molecules in the ground and in excited state and by comparison of the frontier molecular orbitals (HOMO and LUMO), derived from quantum-mechanical calculations (HF, DFT, MP2). Analysis of the results revealed an important influence of non-specific (dispersive) interactions on the solvatochromic behavior of the compounds. 1D and 2D NMR data, *in silico* obtained conformational assembly of the compound, and the NMR analysis of molecular flexibility in solution (NAMFIS), were used to estimate population of conformers and to deconvolute the UV–Vis spectrum of representative derivative; inferring that the conformational assembly is more complex than was assumed in so far published literature data for this class of compounds. Along with this, the emission spectra of the representative compounds were decomposed by the Multivariate Curve Resolution analysis.

© 2014 Elsevier B.V. All rights reserved.

### Introduction

Molecules containing the styryl (arylvinylyl) moiety represent one of the most important groups of functional dyes, with a number of favorable properties. These dyes are fluorescent, have higher

\* Corresponding author. Tel.: +381 11 3303869; fax: +381 11 3370387.

E-mail address: [ntrisovic@tmf.bg.ac.rs](mailto:ntrisovic@tmf.bg.ac.rs) (N.P. Trišović).

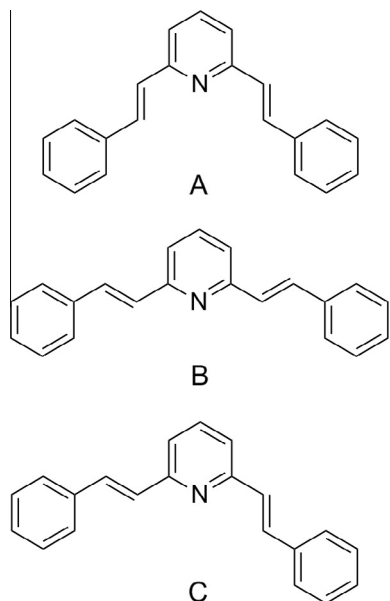


Fig. 1. Schematic representation of preferential conformations of 2,6-distyrylpyridine: *s-cis/s-cis* (A); *s-trans/s-trans* (B); *s-trans/s-cis* (C).

photostability, when compared to classical cyanine dyes, and they can cover the range of the electromagnetic spectrum from the UV to the near infrared region [1]. Styryl dyes are widely used as non-linear optical materials (NLO), optical sensitizers, information recording materials, laser dyes, sensors, two-photon absorption materials, for artificial photosynthesis or photocatalysis [2–6].

2,6-Distyrylpyridine and its derivatives (Fig. 1) have attracted significant attention over the last decade. The physico-chemical properties of these compounds are determined by the existence of the dynamic equilibrium between conformational isomers, which occurs due to the lack of the free rotation of the arylvinyl moieties around the quasi-single bonds with the central pyridine [7]. The preferred conformation of 2,6-distyrylpyridine in solid state is governed by the weak steric interactions between the vinyl hydrogens and the nearby hydrogens of the phenyl or pyridyl rings [8]. *Ab initio* calculations have revealed that among three conformations, conformation A (Fig. 1) is the most stable one, in agreement with the reported crystallographic data. Conformation C is somewhat less stable and conformation B is the least stable [9]. A spectral and photochemical study of 2,6-distyrylpyridine has shown that the relative abundance of different rotamers depends on the solvent used [10]. Its UV–Vis spectra are complex, and reveal the presence of two or three not well-separated electronic transitions. The shape of spectra probably depends on the number and the abundance of rotamers. It is assumed that formation of intramolecular hydrogen bonds stabilizes the sterically favoured, longer lived, rotamer [10].

Pyridinium salts of 2,6-distyrylpyridines exhibit significantly different photophysical properties in comparison with the corresponding neutral forms. Wang et al. have reported that absorption and emission maxima of 2,6-bis(4-dimethylaminostyryl)pyridine are dramatically red shifted upon methylation [11]. They have pointed out that alkylation of the pyridine nitrogen converts this atom to a member of a cyanine array. Increasing the electron-donating ability, number of electron-donating substituents, and the coplanarity of polysubstituted pyridinium molecules is favorable for NLO absorption, especially for saturated absorption at the picosecond pulse [12].

Solvatochromism has been established as an efficient tool to study bulk and local polarity in macrosystems [13–15]. The

solvatochromic comparison methods of Kamlet and Taft [16] and Catalán [17] have been commonly applied to separate effects of non-specific solvent–solute interactions (electrostatic effects) from specific interactions (hydrogen bonding). Recently, it has been demonstrated that a clear and univocal influence of solvent on the position of absorption and fluorescence maxima cannot be obtained using simplified solvation models. A detailed analysis of the static and dynamic aspects of solvation should be taken into account [18].

In this study, we report the set of seven symmetrical 2,6-distyrylpyridines (Fig. 2) substituted with the hydrogen-bond donors and acceptors, bulky hydrophobic moiety and bearing permanently charged fragment. Molecules are able to form hydrogen bonds with the solvent, as well as intramolecular hydrogen bonds, hydrophobic interactions and ion–dipole interactions. Compound 7 is a bent-core mesogen and its liquid crystalline behavior has already been reported [19]. The absorption and emission spectra of the investigated compounds in various solvents have been investigated. Their solvatochromic properties are also described. It is demonstrated that the interpretation of solvent effects on the position of the absorption maxima using both Kamlet–Taft and Catalán models should be taken into consideration cautiously. This is further explained using electrostatic potential of molecules. It is shown that the solvatochromic properties of the investigated molecules originate in greater extent from non-specific solvent–solute interactions (electrostatic effects) than from hydrogen bonding. Furthermore, an analysis of the frontier orbitals and charge distribution, obtained from calculations performed on MP2, DFT and HF level of theory, is described in details.

## Experimental part

### Synthesis

Compounds 1–7 were obtained following the synthetic protocol shown in Scheme 1. Condensation of 2,6-lutidine with the excess of 4-methoxybenzaldehyde in acetic anhydride at the reflux temperature afforded compound 1. Compounds 2–5 were prepared according to the procedure described by Bergmann and Pinchas [20]. Analogously, condensation of 2,6-lutidine with the excess of substituted 4-hydroxybenzaldehydes in acetic anhydride at the reflux temperature gave rise to 2,6-bis[2-(substituted-4-acetoxyphenyl)ethenyl]pyridine. Subsequent base catalyzed hydrolysis led to compounds 2–5. Compound 6 was synthesized in a reaction between *N*-Me-2,6-lutidinium iodide and 4-hydroxybenzaldehyde in the presence of catalytic amount of piperidine. Compound 7 was obtained by acylation of compound 2 with the corresponding 4-*n*-heptyloxybenzoyl chloride. A detailed description of the experimental procedures and the characterization of reported compounds are given in the Supplementary Material.

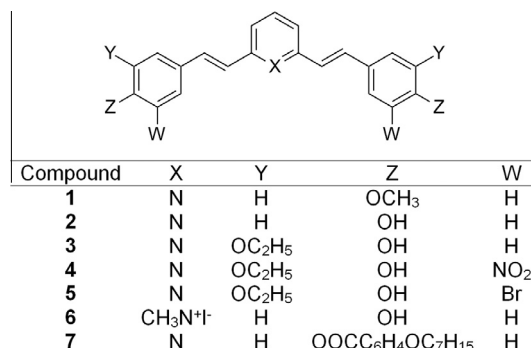
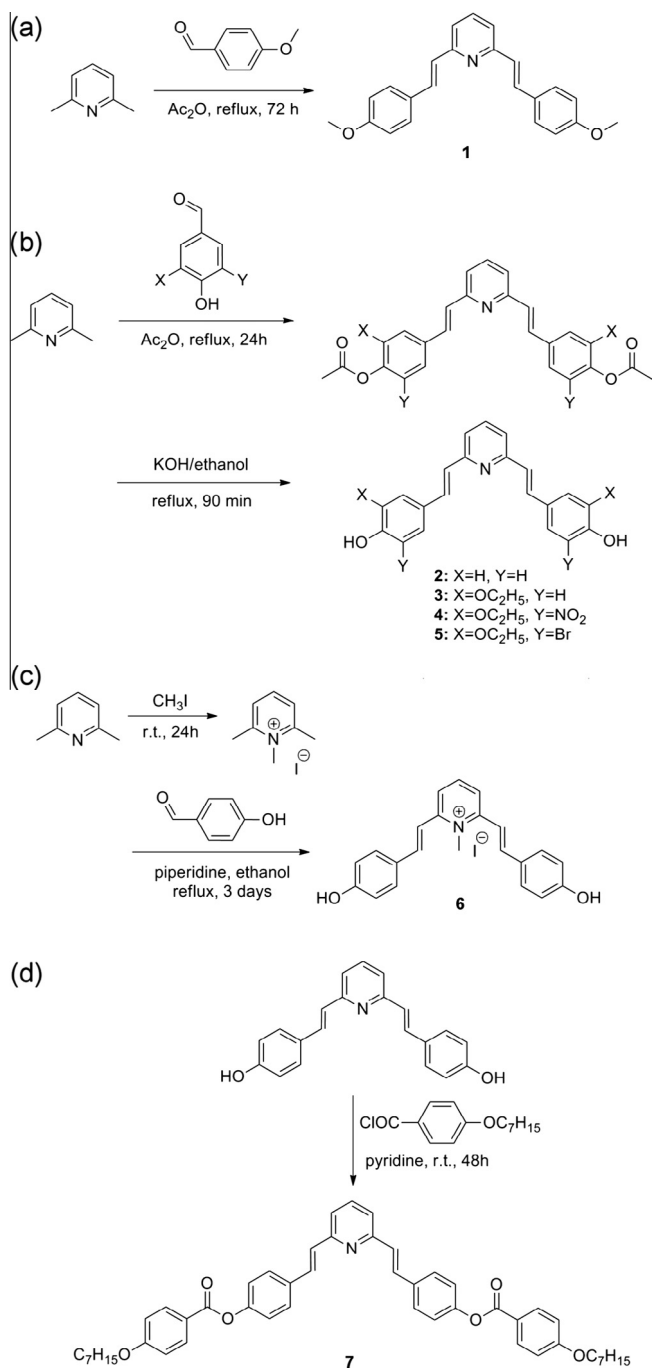


Fig. 2. Schematic depictions of the structure of compounds 1–7.



Scheme 1. Synthetic route to compounds 1–7.

### Spectral measurements

Structures of the synthesized compounds were confirmed by instrumental methods. <sup>1</sup>H and <sup>13</sup>C nuclear magnetic resonance (NMR) spectra were recorded on a Varian Gemini 2000, or Bruker AVANCE 500 instruments, on 200/50, or 500/125 MHz. NMR spectra were recorded in CDCl<sub>3</sub>, or DMSO-*d*<sub>6</sub>, using TMS as the internal standard. Chemical shifts ( $\delta$ ) are reported in ppm. Multiplicities of signals are given as follows: *s* – singlet, *d* – doublet, *t* – triplet, *qu* – quintet, *m* – multiplet. NOESY spectrum of compound 1 in CDCl<sub>3</sub> (7 mg/0.5 mL;  $4.9 \times 10^{-2}$  M) was recorded on Bruker Avance instrument on 500 MHz, with mixing time of 1 s. Fourier-transform infrared spectra (FT-IR) were recorded on a Bomem MB 100 spectrophotometer ( $\nu_{\text{max}}$  are given in cm<sup>-1</sup>) on KBr pellets.

The UV–Vis spectra were recorded using spectroscopy grade solvents (Fluka) at  $1 \times 10^{-5}$  mol dm<sup>-3</sup> concentration, with a Shimadzu 1700 spectrophotometer. Fluorescence spectra of the compounds 1–7 were measured using a Fluorolog-3 spectrofluorimeter (Jobin Yvon Horiba, France) equipped with a 450 W Xe lamp and a photomultiplier tube. The slits on the excitation and emission beams were fixed at 4 nm and 2 nm, respectively. The integration time was 0.1 s. The spectra were corrected for dark counts. Each reported value was average of three scans. All measurements were performed at controlled temperature of 25.0 °C. For the compounds 1–7 emission spectra were measured upon excitation at the wavelength of the absorption maximum in the corresponding solvent. Additionally, for the compounds 2 and 7 series of emission spectra were collected, by excitation at different wavelengths, with a 5 nm-step. The excitation/emission range was 280–450 nm/360–700 nm for the compound 2, and 270–340 nm/350–530 nm for the compound 7. Decomposition of the series of emission spectra was performed using Multivariate Curve Resolution (MCR) [21], in the Unscrambler 9.7 software.

### Computational details

In order to estimate abundance of conformers of compound 1 in CHCl<sub>3</sub> solution, we generated 200 conformers by molecular mechanics conformational search in AMMP program [22]. Boltzmann Jump algorithm was used, with SP4 force field. VegaZZ was used as a GUI [23]. Conformers differing by 10° in any torsion were considered as non-redundant and were included in conformational assembly. Each conformer included in conformational assembly was minimized by SP4 force field, with 20 steps and gradient threshold value of 0.01. Assembly of conformers and NMR data (integrals of NOESY signals and coupling constants, using weight ratio of 1:0.1) were imported in Janocchio program [24], where the input for NAMFIS analysis was prepared. NAMFIS analysis was performed in program DISCO [25]. The initial geometries of all compounds were obtained in MOPAC2012 [26] with PM6 semi-empirical molecular-orbital method [27]. The geometries of three ‘ideal’ conformations of derivative 1 were fully optimized by MP2 method with the 6-311G basis set *in vacuum* in Gaussian03 program [28]. Geometries of all studied molecules were (also) optimized on DFT level of theory, and 6-311G basis set for compounds 1–5 and 7. For compound 6, the DGDZVP basis set was used, because of presence of the iodine in the molecule. Energies of frontier orbitals are derived by self-consistent field analysis of optimized geometries (keyword SCF=tight), for the each case reported. Electrostatic potential of molecules were derived from total SCF density for the ground states, or from total CI density for excited states of molecules, both obtained on HF level of theory with 6-311G basis set. Configuration interactions (CI) calculations were performed considering 30 singlet states. Molecular orbitals are depicted in Jmol [29]. UV–Vis spectra were calculated by semi-empirical ZINDO/S method [30] or by TD-DFT calculations, using implicit solvation in CHCl<sub>3</sub> (IEFPCM – integral equation formalism variant of the polarizable continuum model) in Gaussian09 program [28]. We used equilibrium solvation model for both the ground and the excited states and the default cavitation model (UFF radii scaled by 1.1). Both DFT and TD-DFT calculations were performed with the B3LYP functional. Molecular interaction fields (MIF) around studied molecules were computed using O1 (HBD) and OC2 (HBA) probes of programme GRID [31–33]. Grid resolution was set to 0.5 Å, and rotation of OH groups around C–O axis in response to probes was allowed only (directive MOVE=0). Atomic charges of molecules were calculated by GRID built-in semiempirical method (GRIN directive IHAC=1), in order to retain consistency of GRID methodology.

## Results and discussion

### Solvent effects on the absorption and emission spectra

A preliminary investigation of solvent effects on the absorption maxima shift was performed in solvents with different polarity and hydrogen-bonding ability. A significant shift of the absorption maxima of compound **1** was not observed, while compound **7** appeared insoluble in majority of the solvents used. The solvatochromic behavior of compounds **2–6** was further investigated by recording their absorption spectra in 24 solvents in the spectral range from 200 to 600 nm. The effect of different concentration of the compounds, in the range from  $10^{-4}$  to  $10^{-5}$  mol dm $^{-3}$ , on the position of absorption maxima ( $\lambda_{max}$ ) was also studied. It was observed that variation in concentrations did not influence the position or the shape of absorption bands, confirming that there is no aggregation of the studied compounds in the chosen solvents. The most intensive absorption maxima are shown in Table 1, while representative spectra are shown in Fig. 3a (for compounds **2–6** in methanol) and Fig. 3b (for compound **2** in several typical solvents). As can be seen in Table 1, an increase in solvent polarity shifted the absorption maxima of compounds **2–5** to the longer wavelengths (bathochromic effect). The absorption maxima of the neutral compounds in aprotic solvents are shifted to the shorter wavelengths, in comparison with protic solvents (hypsochromic effect). The reverse situation was observed for compound **6**. Solvents with the highest hypsochromic and bathochromic shifts are marked in Table 1. An unusually large shift of  $\Delta\lambda = 93$ –110 nm for compounds **2–5** in acetic acid is caused by the protonation of the pyridine nitrogen. Because compound **6** is *N*-methylated, a moderate negative solvatochromic shift of  $\Delta\lambda = 35$  nm was observed. Such behavior is characteristic of pyridinium salts [34,35]. Nevertheless, the absorption maxima of the methylated compound **6** undergo a significant bathochromic shift, when compared to the neutral forms.

**Table 1**  
Position of the absorption maxima of compounds **2–6** in selected solvents.

Solvent	Compound				
	2	3	4	5	6
	$\lambda$ (nm)				
1,4-Dioxane	307	329	303	326	439 <sup>c</sup>
Acetonitrile	298 <sup>b</sup>	324 <sup>b</sup>	299	302 <sup>b</sup>	404 <sup>b</sup>
Anisole	306	329	306	325	– <sup>a</sup>
Diethyl ether	302	326	300	309	– <sup>a</sup>
Dichloromethane	299	326	302	308	429
Diisopropyl ether	305	326	298 <sup>b</sup>	309	– <sup>a</sup>
Dimethylacetamide	309	332	307	328	418
Dimethylformamide	308	331	305	327	416
Dimethyl sulfoxide	324	334	306	329	416
Ethyl acetate	304	326	301	309	434
Ethanol	321	348	300	328	417
Ethylene glycol	321	353	360	352	410
Formamide	320	329	382	400	415
Chloroform	300	329	302	323	– <sup>a</sup>
2-Propanol	321	348	300	348	427
Methanol	319	350	301	349	412
1-Butanol	322	349	300	350	428
<i>N</i> -Methylformamide	321	330	387	390	417
1-Propanol	322	350	300	329	425
Pyridine	324	335	310	332	432
Acetic acid	408 <sup>c</sup>	420 <sup>c</sup>	391 <sup>c</sup>	410 <sup>c</sup>	406
<i>tert</i> -Butanol	321	343	300	345	434
Tetrahydrofuran	306	331	302	327	438
Toluene	307	328	306	324	– <sup>a</sup>
$\Delta\lambda$ (nm)	110	96	93	108	35

<sup>a</sup> Insoluble in given solvent.

<sup>b</sup> Solvent with the highest hypsochromic shift.

<sup>c</sup> Solvent with the highest bathochromic shift.

The experimentally obtained fluorescence and absorption maxima and the corresponding Stokes shifts ( $\Delta\lambda_s$ ) of compounds (**2–6**) measured in six solvents are shown in Table 2. The fluorescence spectra of all compounds in methanol and the fluorescence spectra of compound **2** in selected solvents are shown in Fig. 4a and b, respectively. With increasing solvent polarity, both absorption and emission maxima undergo a bathochromic shift, the latter being more pronounced than the former, except for the compound **4**. Furthermore, the emission spectra in polar solvents (methanol, formamide) are broad and structureless, when compared with spectra recorded in less polar solvents (e.g. ethyl acetate). This indicates the formation of an ICT state rapidly after the excitation [36]. The methylated compound **6** has emission maxima at longer wavelengths than the neutral compounds (Fig. 4a), but the smallest shift of the absorption and the fluorescence maxima was observed in the solvents used, compared to neutral compounds (Table 2). Thus, the Stokes shift values for compounds **2–6** increase with the solvent polarity, implying that their dipole moment is larger in the excited state than in the ground state ( $\mu_e > \mu_g$ ).

### Conformational assembly of compound **1**

The shape of the UV–Vis spectra of 2,6-distyrylpyridines and structurally similar compounds are commonly ascribed to simultaneous existences of a few rotamers in solution. This phenomenon has been examined using different spectroscopic techniques [37], mostly fluorescent. Literature reports on NMR investigation of rotamerism of 2,6-distyrylpyridines and similar compounds are not frequent, most probably because inherent time-scale of nuclear transition, as well as relatively low sensitivity of the method. On the other hand, conformational preferences of flexible molecules in solution have been frequently examined by NMR [38,39]. NMR spectra of flexible molecules represent an average conformation of the compound, due to the fast conformational exchange during time scale of spectrum recording. Such average conformation, most often, does not correspond to the conformation of any real conformer that exists in solution. NAMFIS analysis [24] was tailored to resolve structures and the relative populations of several conformers from the NMR data and the conformational assemblies of studied molecules.

We aimed to estimate population of rotamers of compound **1** in chloroform using  $^1\text{H}$  NMR and NOESY spectra and NAMFIS analysis. Compound **1** was chosen because of well-resolved NOESY signals in its spectrum recorded in chloroform. Afterwards, the UV–Vis spectra of the most abundant rotamers, as found by NAMFIS analysis, were calculated and compared with the experimentally obtained UV–Vis spectrum of compound **1** in  $\text{CHCl}_3$ . The section of the  $^1\text{H}$  NMR spectrum of compound **1** in chloroform that corresponds to the aromatic and vinylic protons, is shown in Fig. 5.

All NMR signals are well-resolved, and coupling constants of 16.02 Hz unambiguously show the *trans*-configuration of the vinylic bonds (7.07 and 7.65 ppm). Only pattern of the 4-MeO–Ph AB protons (6.92 and 7.55 ppm) point to few rotamers around Ph–CH=CH– bonds. NOESY signal between 4-MeO–hydrogens and Ph AB protons, unambiguously show that the doublet on 6.92 ppm belongs to protons on Ph ring in *ortho*-position to MeO–group (Fig. 6a). From the section of NOESY spectrum from 6.80 to 7.30 ppm, the spatial vicinity of the proton of –CH=CH– moiety at 7.65 ppm and both the *meta*-pyridine hydrogens and the phenyl hydrogens *ortho*- to vinyl bond was obvious (Fig. 6b). On the other hand, the protons of the –CH=CH– moiety at 7.08 ppm are close to the phenyl hydrogens *ortho*- to the vinyl bond. So, average conformation of molecule appeared very different from three conformations shown in Fig. 1, which have been found as the local minima obtained by geometry optimization on high level of theory

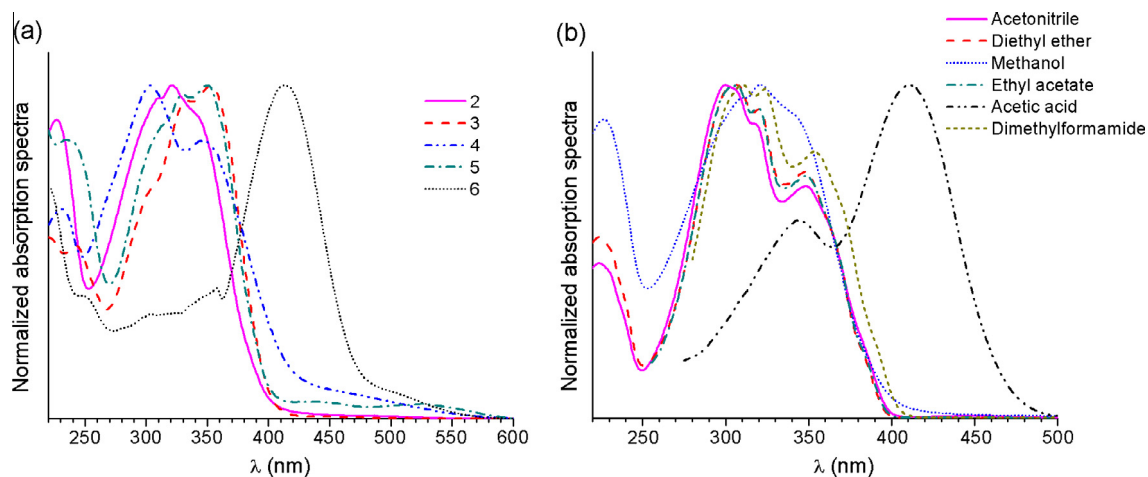


Fig. 3. Representative UV-Vis spectra. Normalized absorption spectra of: (a) compounds 2–6 in methanol, and (b) compound 2 in selected solvents.

Table 2

Absorption and fluorescence maxima, and the Stokes shift ( $\Delta\lambda_s$ , given in bold) of compounds 2–6 in selected solvents.

Compound	Solvent							$\Delta\lambda$ (nm)
		ACN <sup>a</sup>	EtOAc <sup>b</sup>	Chloroform	DMA <sup>c</sup>	MeOH <sup>d</sup>	Formamide	
2	$\lambda_{max}^{Abs}$ (nm)	298	304	300	309	319	320	22
	$\lambda_{max}^{Fluor}$ (nm)	408	397	407	411	435	443	46
	$\Delta\lambda_s$ (nm)	<b>110</b>	<b>93</b>	<b>107</b>	<b>102</b>	<b>116</b>	<b>123</b>	
3	$\lambda_{max}^{Abs}$ (nm)	324	326	329	332	350	329	26
	$\lambda_{max}^{Fluor}$ (nm)	425	404	412	434	446	444	42
	$\Delta\lambda_s$ (nm)	<b>101</b>	<b>78</b>	<b>83</b>	<b>102</b>	<b>96</b>	<b>115</b>	
4	$\lambda_{max}^{Abs}$ (nm)	299	301	302	307	301	382	83
	$\lambda_{max}^{Fluor}$ (nm)	407	399	405	478	401	445	79
	$\Delta\lambda_s$ (nm)	<b>108</b>	<b>98</b>	<b>103</b>	<b>171</b>	<b>100</b>	<b>63</b>	
5	$\lambda_{max}^{Abs}$ (nm)	302	309	323	328	349	400	98
	$\lambda_{max}^{Fluor}$ (nm)	421	399	410	414	422	516	117
	$\Delta\lambda_s$ (nm)	<b>119</b>	<b>90</b>	<b>87</b>	<b>86</b>	<b>73</b>	<b>116</b>	
6	$\lambda_{max}^{Abs}$ (nm)	404	434	– <sup>e</sup>	418	412	415	30
	$\lambda_{max}^{Fluor}$ (nm)	514	516	– <sup>e</sup>	509	517	479	38
	$\Delta\lambda_s$ (nm)	<b>110</b>	<b>82</b>	–	<b>91</b>	<b>105</b>	<b>64</b>	

<sup>a</sup> Acetonitrile.

<sup>b</sup> Ethyl acetate.

<sup>c</sup> Dimethylacetamide.

<sup>d</sup> Methanol.

<sup>e</sup> Insoluble in given solvent.

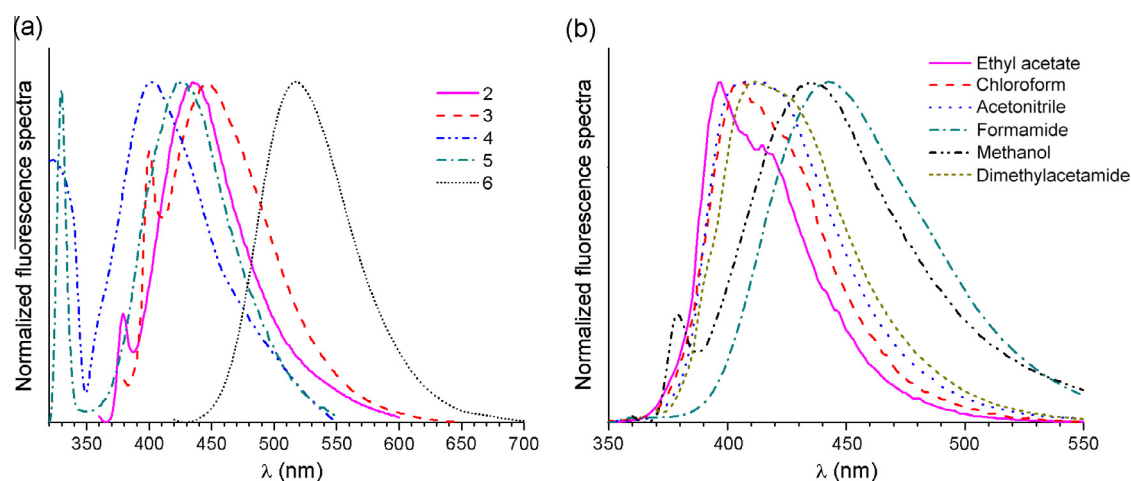


Fig. 4. Representative fluorescence spectra. Normalized fluorescence spectra of: (a) compounds 2–6 in methanol, and (b) compound 2 in selected solvents.

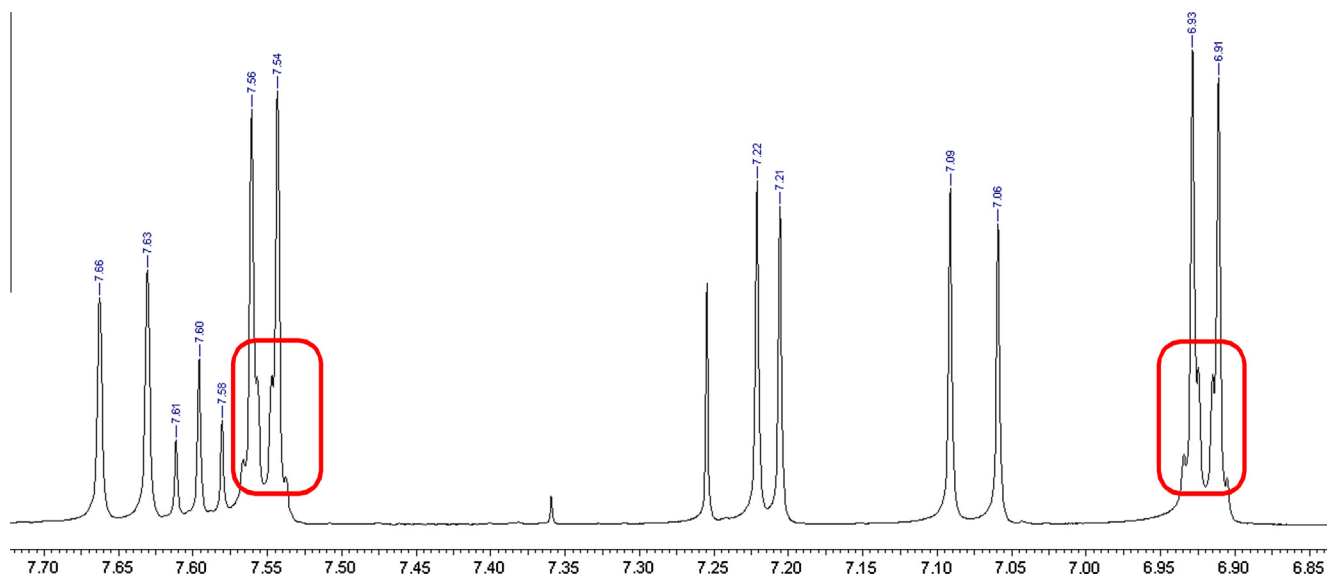


Fig. 5. The section of the  $^1\text{H}$  NMR spectrum of compound **1** in chloroform that include signals of the aromatic and vinylic protons.

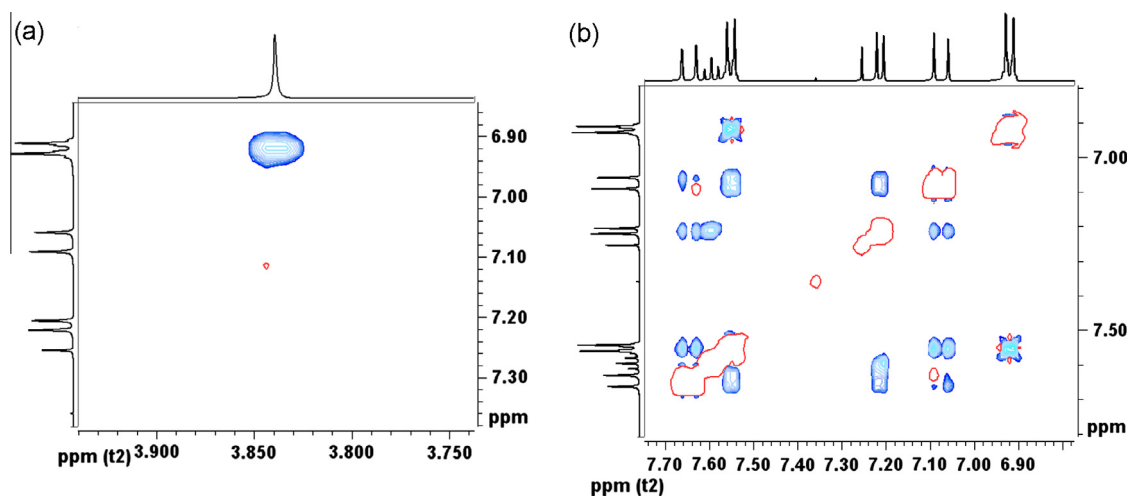


Fig. 6. The sections of the  $^1\text{NOESY}$  spectrum of compound **1**: (a) signal between 4-MeO—protons and protons of the phenyl ring in *ortho*-position to MeO— group; (b) signals of aromatic and vinylic protons.

(HF, DFT and MP2) [9], for structurally similar 2,6-distyrylpyridine derivative.

NAMFIS analysis recognized three conformers as the most abundant ones (Fig. 7, I–III). Those three conformers accounts for 91% of all conformers in solution. We normalized abundance of those three conformers to 100%. An UV–Vis spectrum of each conformer is calculated by the ZINDO/S method [30], and the intensities of obtained spectra were scaled according to abundance of conformers found by NAMFIS analysis. The overlapped, calculated, UV–Vis spectra are shown in Fig. 8.

The calculated UV–Vis spectra of the most abundant conformers derived from NOESY data and NAMFIS analysis are in obvious disagreement when compared to the experimentally obtained UV–Vis spectrum of derivative **1** in  $\text{CHCl}_3$ . One of the possible reasons for this is difference in concentrations of the NMR and the UV–Vis samples. NMR spectra of derivative **1** are recorded in concentration of  $4.9 \times 10^{-2}$  M, while the UV–Vis spectrum is recorded in concentration of  $1 \times 10^{-5}$  M. Next, we used symmetrically substituted compound, so in  $^1\text{H}$  NMR spectrum only one pair of doublets for both vinylic bonds and for aromatic protons of the Ph moieties appeared. Although we treated derivative **1** as unsymmetrical

during data preparation for NAMFIS analysis, i.e. coupling constants and NOESY signals were assigned to each Ph–CH=CH— moiety, and only the protons of the MeO–methyl group were considered as equivalent, more accurate structure–spectra assignment will be assessed for unsymmetrically substituted derivatives. For example, see reference [40] where NMR spectra of unsymmetrically substituted derivatives was described.

The positions of absorption maxima at  $\sim 320$  and  $340$  nm in the calculated and experimentally obtained UV–Vis spectra are in fair agreement (Fig. 8). The most red-shifted peak in calculated UV–Vis spectrum (conformer I,  $\nu_{\text{max}} = 340$  nm calculated; observed 348 nm for the most red-shifted peak in the experimentally obtained spectrum) are significantly broader, comparing to the most red-shifted peak in the experimentally obtained UV–Vis spectrum. In this conformation (I), Ph— to —CH=CH— torsion of  $\sim 85^\circ$  in one of the styryl fragments was found, while the same torsions is significantly lower in the other styryl part. This conformation in —CH=CH—Py—CH=CH— part roughly resembles conformation A depicted in Fig. 1 (*s-cis/s-cis*). The peak in the calculated spectra of conformation III is blue-shifted with respect to the real spectrum ( $\nu_{\text{max}} = 284$  nm calculated, observed 308 nm for the most

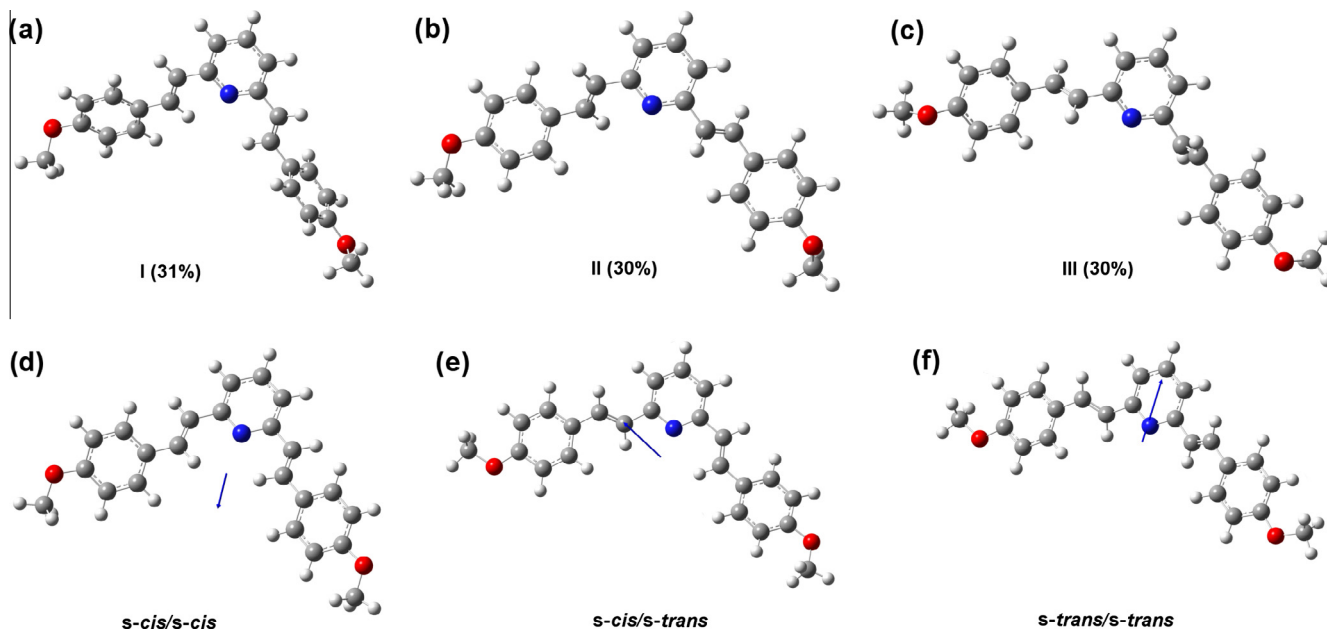


**Fig. 7.** (a–c) The most abundant conformers of compound **1** in  $\text{CHCl}_3$  solution, as found by NOESY data and NAMFIS analysis. (d–f) Local minima of compound **1** with different geometries of  $\text{Py}-\text{CH}=\text{CH}$  bonds, obtained by MP2 calculations. Dipoles are also shown. For clarity, the dipole of *s-trans/s-trans* conformer (f) is scaled with 0.85.

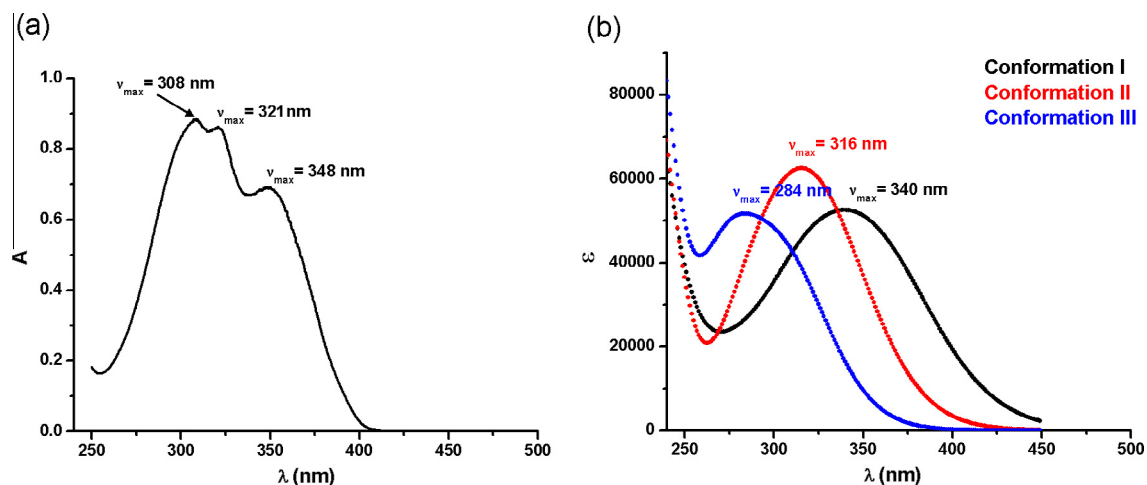


**Fig. 8.** (a) Experimentally obtained UV-Vis spectrum of compound **1** in chloroform; (b) calculated UV-Vis spectra of conformers **I–III** shown in Fig. 7a–c.

blue-shifted peak in the experimentally obtained spectrum) and this peak is (again) significantly broader than in the experimentally obtained UV-Vis spectrum. In this conformation  $\text{Py}-$  to  $-\text{CH}=\text{CH}-$  torsion of  $\sim 83^\circ$ , and the  $\text{Ph}-$  to  $-\text{CH}=\text{CH}-$  torsion of  $\sim 48^\circ$  in one styryl fragment were found, while in other  $\text{Ph}-$  to  $-\text{CH}=\text{CH}-$  torsion is of  $\sim 41^\circ$ . This conformation in  $-\text{CH}=\text{CH}-\text{Py}-\text{CH}=\text{CH}-$  part roughly resembles conformation **B** depicted in Fig. 1 (*s-trans/s-trans*). The only conformation with the fairly predicted UV-Vis spectrum is conformation **II**, with the calculated absorption maximum at 316 nm (the experimentally obtained absorption maximum of the ‘middle’ peak was at 321 nm). Although in this conformation both  $\text{Py}-$  to  $-\text{CH}=\text{CH}-$  and  $\text{Ph}-$  to  $-\text{CH}=\text{CH}-$  torsions appeared significant (different from *almost coplanar* ‘ideal’ conformations schematically depicted in Fig. 1), such conformation is less symmetrical in  $-\text{CH}=\text{CH}-\text{Py}-\text{CH}=\text{CH}-$  part, comparing to conformations **I** and **III**. So, the calculated UV-Vis spectrum of conformation **II**, which most resemble conformation having *s-cis* configuration in the one styryl part and the *s-trans* configuration

in the other styryl part, appeared closest to the middle part of experimentally obtained spectrum of compound **1** in  $\text{CHCl}_3$ , both by the position of absorption maximum and by the width of the absorption peak. Most probably, other two conformations that fit to absorption maxima (and peak widths) at 308 and 348 nm in experimentally obtained spectrum of compound **1** in  $\text{CHCl}_3$  can be found among similar conformations having *s-cis* configuration in the one styryl part and the *s-trans* configuration in the other. HOMO  $\rightarrow$  LUMO and HOMO  $\rightarrow$  LUMO+1 transitions contribute mainly to absorption peaks at 340 and 316 nm of conformations **I** and **II**, respectively; while HOMO  $\rightarrow$  LUMO and HOMO-1  $\rightarrow$  LUMO+2 transitions contribute to the absorption peak on 284 nm of conformation **III**. Those molecular orbitals are shown in Fig. S1 in Supplementary Material.

In order to further examine hypothesis of preferred conformers of compound **1** in  $\text{CHCl}_3$ , we optimized geometry of compound **1** in three ‘ideal’ conformations, schematically depicted in Fig. 1, to stationary points (local minima) by MP2 calculations and 6-311G

basis set *in vacuum* (Fig. 7d–f). Vibration analysis showed that no imaginary frequencies exist, confirming that local minima were obtained. Predicted thermal energy and zero-point vibrational energies of conformers, energies of frontier orbitals and numerical values of dipoles are shown in Table 3. Dipoles are also depicted in Fig. 7. It should be noted that for the 4-MeO-substituted derivative (**1**) significantly lower differences in energies of three conformers were obtained, comparing to data reported in Ref. [9], obtained for the unsubstituted compound. This can be a consequence of somewhat different structures of compounds, as well as the differences in basis sets used.

The UV–Vis spectra of all conformations obtained by MP2 method were calculated by semiempirical ZINDO/S method, and by TD-DFT calculations with 6-311G basis set. The calculated UV–Vis spectra are shown in Supplementary Material (Fig. S2). Obviously, the predicted UV–Vis spectra obtained by ZINDO/S method are (at least by the position of the absorption maxima) something more like to the experimentally obtained spectrum of compound **1**, but are still in significant extent far from the real spectrum, considering both the width of the peaks and the positions of absorption maxima. A more detailed examination of this type will be performed on unsymmetrically substituted derivatives in future.

#### Nature of the frontier molecular orbitals

The optimized molecular geometries, their highest occupied molecular orbitals (HOMOs) and lowest unoccupied molecular orbitals (LUMOs) are shown in Fig. 9.

The molecular geometries of neutral compounds **1–5** and **7**, are optimized in their *s-cis/s-cis* geometries to stationary point, on DFT level of theory (B3LYP/6-311G). Energies of frontier orbitals are shown in Table 4. Qualitatively, HOMO of the neutral compounds is delocalized over the entire molecule, while, with the exception of compounds **4** and **7**, LUMO is shifted towards the central pyridine ring. The introduction of the weakly electron-donating ethoxy groups in compounds **3** and **5** does not produce any appreciable change in the position of HOMO and LUMO orbitals with respect to compound **2**. The energy gap of these compounds resembles that of compound **2**, although the involvement of the oxygen atoms in HOMO slightly lowers its energy. On the other hand, the introduction of the strong electron-withdrawing nitro group in compound **4** causes a shift of the electron density of LUMO towards the outer phenyl rings. LUMO and LUMO+1 orbitals are almost degenerated for compound **4** (Fig. 9 and Table 4). In addition, the introduction of the nitro group leads to a stronger stabilization of both HOMO and LUMO orbitals, and the energy gap for this compound is the lowest, when compared with other neutral compounds. It should be noted that the magnitude of dipole moment of the neutral compounds increases with increasing number of substituents in the outer rings, and the electron-withdrawing ability of substituents (Table 4). In compound **7**, which is symmetrical as the other compounds, both LUMO and LUMO+1 orbitals are delocalized over its bent core in something unsymmetrical fashion, and energies of both HOMO and LUMO are lowered with respect to compound **2**.

As a consequence of *N*-methylation of the central pyridine ring, and the presence of the iodine counter-ion, the *s-cis/s-trans* conformation of compound **6** was found as the most stable. The HOMO orbital is delocalized over the whole system, while LUMO is primarily located on the styrylpyridinium core with minimal density on the iodide counter anion. Because basis set used for compound **6** is different from the basis set used for geometry optimization of the neutral compounds, energies of the frontier orbitals and their difference for this compound cannot be compared with the rest in the set.

#### Linear solvation energy correlation analyses

The Kamlet–Taft [16] and Catalán [17] linear solvation energy relationship (LSER) models were used in order to investigate effects of solvent–solute interactions on the absorption maxima shifts (solvatochromic properties). The three-parameter Kamlet–Taft model (Eq. (1)) describes hydrogen bond donating ( $\alpha$ ) and hydrogen bond accepting ( $\beta$ ) capacities, along with dipolarity/polarizability ( $\pi^*$ ) of solvents.

$$\tilde{\nu}_{max} = \tilde{\nu}_{max,0} + a \cdot \alpha + b \cdot \beta + s \cdot \pi^* \quad (1)$$

The significance of each of those effects on the solvatochromic properties is expressed by the weights of terms *a*, *b* and *s*. Although this is the most frequently used LSER model, it does not separate dipolarity and polarizability effects of solvents. The newer, Catalán LSER model (Eq. (2)), provides different parameters, *SP* and *SdP*, for those two effects, respectively, along with parameters which describe hydrogen bond donating (*SA*) and hydrogen bond accepting (*SB*) abilities of solvents.

$$\tilde{\nu}_{max} = \tilde{\nu}_{max,0} + a \cdot SA + b \cdot SB + c \cdot SP + d \cdot SdP \quad (2)$$

The solvent parameters of both models are given in Supplementary Material (Table S1). The results of the multiple linear regression analysis obtained by the Kamlet–Taft and Catalán models are shown in Tables 5 and 6, respectively. All correlation coefficients (*R*) calculated at the 95% confidence level are higher than 0.91, for all regressions. Therefore, those equations are suitable for the analysis of solvatochromic behavior. The success of the quantification and interpretation of solvent effects on the position of the most intense absorption band is illustrated in Fig. S3 (Supplementary Material) by plots of  $\nu_{max}$  measured ( $\nu_{exp}$ ) versus  $\nu_{max}$  calculated ( $\nu_{calc}$ ).

In both models, coefficient *a* provides information about interactions between hydrogen-bond donating (HBD) moiety of solvents and the appropriate hydrogen-bond accepting (HBA) fragments of compounds, while coefficient *b* describes the specific solvation of compounds by hydrogen bonding to the HBA moieties of solvents.

One can expect that HBD solvents interact with the pyridine nitrogen, or with the oxygen atoms of OH, EtO or NO<sub>2</sub> groups of molecules, but the strength of such interactions are different from compound to compound. The accessibility and the strength of interactions of the hydrogen-bonding moieties of the molecules, in their ground state, with HBA and HBD were estimated using GRID [31–33] probes that represent the hydroxyl group bound to

**Table 3**  
Predicted stabilities, energies of frontier orbitals and dipoles of three conformers of 4-MeO derivative (**1**), Fig. 7d–f, as obtained by MP2 calculations with 6-311G basis set on *T* = 298.16 K and *P* = 1 atm, without applied solvent model.

Conformer	Thermal <i>E</i> (kcal/mol)	Zero-point vibrational <i>E</i> (kcal/mol)	<i>E</i> HOMO (Hartree)	<i>E</i> LUMO (Hartree)	Dipole (Debye)
<i>s-trans/s-trans</i>	250.597	235.272	−0.27507	0.07087	4.528
<i>s-cis/s-trans</i>	249.642	234.739	−0.27290	0.07100	2.674
<i>s-cis/s-cis</i>	250.233	234.783	−0.27184	0.06877	2.289

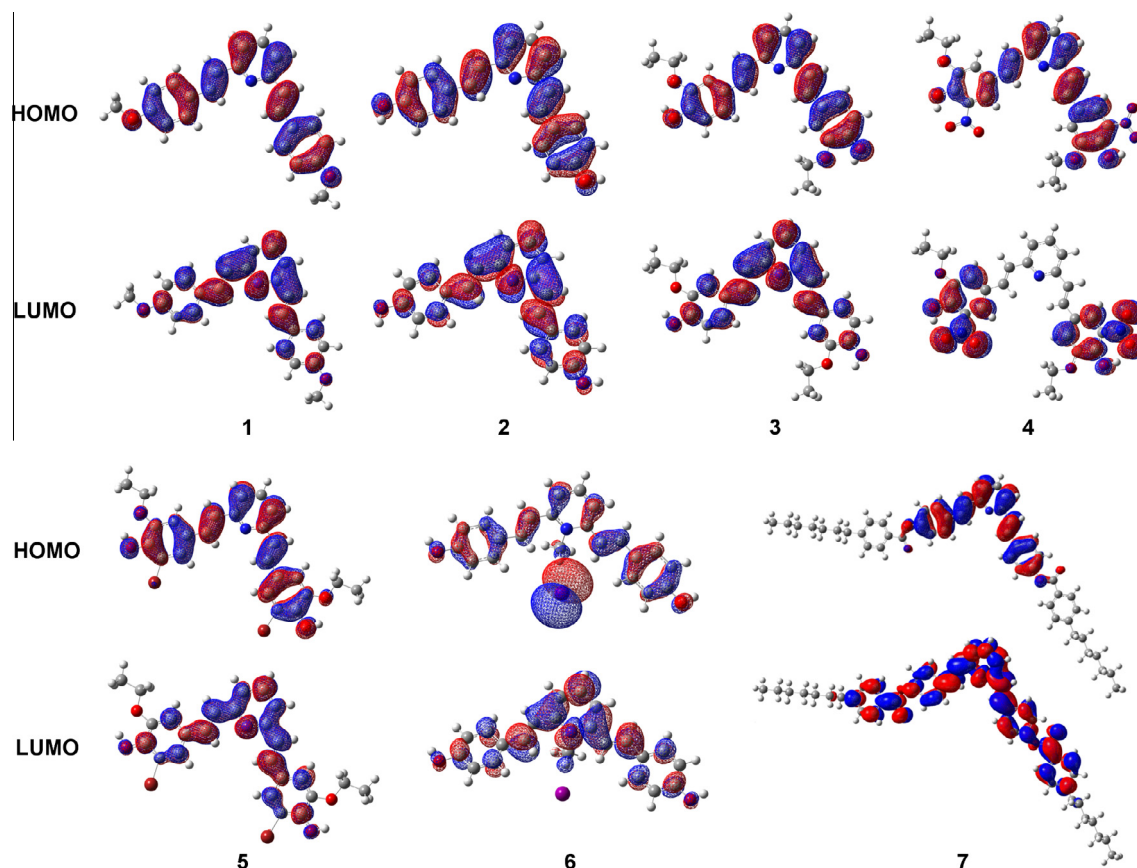


**Fig. 9.** HOMO and LUMO orbitals of compounds 1–7, as obtained by DFT calculations. LUMO and LUMO+1 orbitals of compounds 4 and 7 are almost symmetrical in respect to plane defined by the N and the C4 atom of the pyridine ring. Both LUMO and LUMO+1 are depicted for those compounds.

**Table 4**

Energies of frontier molecular orbitals and their difference,  $E$  gap, dipoles and Mülliken charges at the pyridine N of compounds 1–5 and 7.

Compound	$E$ HOMO (Hartree)	$E$ LUMO (Hartree)	$E$ gap (Hartree) <sup>a</sup>	Dipole (Debye)	Mülliken charge at pyridine N (a.u.) <sup>b</sup>
1	−0.19881	−0.06032	0.13849	1.823	−0.4187
2	−0.20250	−0.06288	0.13962	2.004	−0.4188
3	−0.20281	−0.06265	0.14016	4.152	−0.4198
4	−0.22270	−0.12715 (−0.12320) <sup>c</sup>	0.09555	8.176	−0.4192
5	−0.20622	−0.06987	0.13635	10.257	−0.4177
7	−0.20923	−0.07246 (−0.06945) <sup>c</sup>	0.13677	2.166	−0.4161

<sup>a</sup>  $E$  gap is difference in energies of HOMO and LUMO orbitals.

<sup>b</sup> Atomic units.

<sup>c</sup> LUMO+1. For compounds 4 and 7, we found very similar energies of LUMO and LUMO+1 orbitals, which are almost degenerated. In compound 4, LUMO orbital covers one half of the molecule, while LUMO+1 orbital cover the other half. In compound 7, both LUMO and LUMO+1 orbitals in something unsymmetrical fashion cover  $-C(O)O-Ph-CH=CH-Py-CH=CH-Ph-O(O)C-$ , but are mutually symmetrical. Because of this, both LUMO and LUMO+1 orbitals of compounds 4 and 7 are shown in Fig. 9.

**Table 5**

Regression data ( $\pm$ sd) for the Kamlet–Taft model.

Compound	$\nu_0$ (cm <sup>−1</sup> )	$a$	$b$	$s$	$R^a$	$sd^b$ (cm <sup>−1</sup> )	$F^c$	sign. $F^c$	$n^d$
2	34,374 ( $\pm$ 344)	−1114 ( $\pm$ 255)	−2137 ( $\pm$ 338)	−1035 ( $\pm$ 403)	0.924	396	32.9	$<1 \times 10^{-6}$	21 <sup>e</sup>
3	31,337 ( $\pm$ 237)	−1741 ( $\pm$ 179)	−1092 ( $\pm$ 225)	−586 ( $\pm$ 299)	0.958	274	62.5	$<1 \times 10^{-8}$	21 <sup>f</sup>
4	32,065 ( $\pm$ 962)	−4259 ( $\pm$ 634)	7132 ( $\pm$ 1216)	−5014 ( $\pm$ 856)	0.945	811	30.4	$<1 \times 10^{-4}$	15 <sup>g</sup>
5	33,453 ( $\pm$ 594)	−2481 ( $\pm$ 450)	−2152 ( $\pm$ 576)	−1760 ( $\pm$ 718)	0.910	646	20.9	$<1 \times 10^{-4}$	17 <sup>h</sup>
6	21,999 ( $\pm$ 484)	1238 ( $\pm$ 249)	−1094 ( $\pm$ 432)	2932 ( $\pm$ 534)	0.886	326	13.4	$<5 \times 10^{-4}$	15 <sup>i</sup>

<sup>a</sup> Correlation coefficient.

<sup>b</sup> Standard deviation.

<sup>c</sup> Fisher test of significance.

<sup>d</sup> Number of solvents.

<sup>e</sup> Excluded solvents: acetic acid, pyridine, toluene.

<sup>f</sup> Excluded solvents: acetic acid, *N*-methylformamide, formamide.

<sup>g</sup> Excluded solvents: acetic acid, dichloromethane, methanol, chloroform, *N*-methylformamide, acetonitrile, anisole, toluene, ethanol.

<sup>h</sup> Excluded solvents: acetic acid, toluene, ethanol, 1-propanol, acetonitrile, formamide, *N*-methylformamide.

<sup>i</sup> Excluded solvents: dichloromethane, formamide, ethylene glycol, pyridine. Insoluble in: anisole, diethyl ether, diisopropyl ether, chloroform, toluene.

**Table 6**  
Regression data ( $\pm$ sd) for the Catalán model.

Compound	$\nu_0$ (cm <sup>-1</sup> )	<i>a</i>	<i>b</i>	<i>c</i>	<i>d</i>	<i>R</i> <sup>a</sup>	<i>sd</i> <sup>b</sup> (cm <sup>-1</sup> )	<i>F</i> <sup>c</sup>	sign. <i>F</i> <sup>c</sup>	<i>n</i> <sup>d</sup>
<b>2</b>	35,603 ( $\pm$ 1032)	-2796 ( $\pm$ 378)	-2480 ( $\pm$ 410)	-2871 ( $\pm$ 1297)	614 ( $\pm$ 374)	0.950	322	34.4	$<1 \times 10^{-6}$	20 <sup>e</sup>
<b>3</b>	32,582 ( $\pm$ 628)	-3971 ( $\pm$ 359)	-1597 ( $\pm$ 247)	-2326 ( $\pm$ 812)	443 ( $\pm$ 252)	0.975	211	66.2	$<1 \times 10^{-8}$	19 <sup>f</sup>
<b>4</b>	43,326 ( $\pm$ 2467)	-5726 ( $\pm$ 1004)	5876 ( $\pm$ 1740)	-24,002 ( $\pm$ 3750)	4440 ( $\pm$ 1491)	0.935	892	19.1	$<1 \times 10^{-4}$	16 <sup>g</sup>
<b>5</b>	41,979 ( $\pm$ 2227)	-8407 ( $\pm$ 1182)	-3199 ( $\pm$ 981)	-13,525 ( $\pm$ 2904)	1340 ( $\pm$ 967)	0.914	843	18.9	$<1 \times 10^{-5}$	20 <sup>h</sup>
<b>6</b>	24,077 ( $\pm$ 760)	771 ( $\pm$ 273)	-1682 ( $\pm$ 405)	-1880 ( $\pm$ 952)	2263 ( $\pm$ 384)	0.931	265	19.4	$<1 \times 10^{-4}$	17 <sup>i</sup>

<sup>a</sup> Correlation coefficient.<sup>b</sup> Standard deviation.<sup>c</sup> Fisher test of significance.<sup>d</sup> Number of solvents.<sup>e</sup> Excluded solvents: *N*-methylformamide, acetic acid, pyridine, dimethyl sulfoxide.<sup>f</sup> Excluded solvents: *N*-methylformamide, acetic acid, formamide, ethylene glycol, diisopropyl ether.<sup>g</sup> Excluded solvents: *N*-methylformamide, chloroform, anisole, toluene, dichloromethane, 1,4-dioxane, acetic acid, pyridine.<sup>h</sup> Excluded solvents: *N*-methylformamide, acetic acid, ethylene glycol, 1-propanol.<sup>i</sup> Excluded solvents: *N*-methylformamide, dichloromethane. Insoluble in: anisole, diethyl ether, diisopropyl ether, chloroform, toluene.

an aliphatic alkyl chain (HBD probe) and the aliphatic ether oxygen (HBA probe). The set of the solvents used for the experimental evaluation of solvatochromic properties of the studied molecules comprises a number of aliphatic alcohols and ethers. MIFs depicted on isocontour levels of  $-4.5$  kcal/mol for HBD probe, and  $-2.0$  kcal/mol for HBA probe are shown in Fig. S4 in Supplementary Material. The steric hindrance of the pyridinium nitrogen with the  $-\text{CH}=\text{CH}-$  moieties for interaction with HBD probe is obvious. Interactions of the 'lone' OH groups on the outer phenyl moieties in compound **2** with HBD probe is of significantly lower strength than the interactions of proximal EtO and OH; or EtO, NO<sub>2</sub> and OH groups in compounds **3–5**. For compound **2**, interactions with HBD probe is depicted on isocontour level of  $-3.8$  kcal/mol, in order that MIF be visible. It should be noted that HBD probe exerts significantly weaker interactions with the NO<sub>2</sub> group of compound **4**. MIF of HBD probe associated with the NO<sub>2</sub> group is visible on isocontour level of  $\sim -3.5$  kcal/mol (data not shown). The ester carbonyl O exerts stronger interactions with HBD probe than ester  $-\text{C}(\text{O})\text{Q}-$ , in chosen conformation, most probably due to the steric hindrance of this oxygen by the vicinal phenyl rings.

The charge distribution in the ground state of the molecules significantly changes upon introduction of different substituents in the outer phenyl rings. This is illustrated by the graphical depiction of the negative lobe of the electrostatic potential (ESP) of compounds **1–5**, **7** in the ground state, obtained from total self-consistent field (SCF) density (Fig. 10). Surfaces are depicted on arbitrary chosen isocontour level, which provide good distinction among the compounds studied; and negative lobe of ESP was chosen, because it covers moieties of all heteroatoms in molecules, which participate in (intermolecular) hydrogen bonding. Such differences cannot be observed by considering the calculated atomic charges on, for example, the pyridine nitrogen (see Table 4) or on any other heteroatom in the molecules. Along with this, the frontier molecular orbitals (HOMO and LUMO), depicted in Fig. 9, provide a different kind of information. In this place, it should be noted that electrostatic potential of a molecule is a physical observable, while atomic charges and molecular orbitals are not. In the case of compound **4**, most probably, the formation of a strong intramolecular hydrogen bond between the nitro and hydroxyl groups efficiently hinders HBD ability of the OH group to solvent, resulting in a positive sign of coefficient *b*. In the case of compound **5**, halogen bonding of bromine with HBA of solvents should also be considered [41].

Difference in charge distribution of compounds in the ground and in excited state can be clearly seen in Fig. 10. For all compounds, negative lobe of ESP covers a greater part of the pyridine moiety in the excited state, when compared to the ground state of the molecule. The lowest difference can be observed for

compound **1**, which did not exert observable solvatochromism. For compound **4**, the largest difference in negative lobes of electrostatic potential in the ground and excited state can be observed on the one of NO<sub>2</sub> groups. All described is consistent with the regression coefficients derived from the Kamlet–Taft and Catalán models. Both terms associated with the HBD and HBA influence of solvent (*a* and *b*) are of the same sign (except term *b* for compound **4**, as explained above) and have relative low variation from compound to compound. Both Kamlet–Taft coefficient *s* and Catalán coefficient *c* showed largest variability. So, the solvatochromic behavior of compounds **2–6** can be in a considerable extent ascribed to non-specific electrostatic interactions with the solvent, rather than to specific hydrogen bonding. Most probably that such behavior stems from the high symmetry of the investigated compounds. Considering the Catalán model, it can be seen that the magnitude of the polarizability (coefficient *c*) is higher than that of the dipolarity (coefficient *d*). Most probably because of the presence of electron-withdrawing substituents (NO<sub>2</sub> and Br), the highest values of coefficient *d* was obtained for compounds **4** and **5**, which also have the largest dipole moments in the ground state (Table 4). A hypsochromic shift with increasing solvent dipolarity/polarizability (positive *s* coefficient) is observed for compound **6**.

#### Multivariate Curve Resolution (MCR) analysis

The emission spectra of compounds **2** and **7** were compared in order to analyze effect of esterification of the hydroxyl group of compound **2** on the position of emission maxima and the complexity of the spectra.

The series of emission spectra of the compounds **2** and **7** in chloroform, as well as the results of corresponding MCR analysis of the emission profiles are shown in Fig. 11. The emission spectra of compound **2** contain five components with the emission maxima positioned at 392, 415, 480, 518 and 553 nm. The spectrum of compound **7** contains four components with the maxima at 380, 394, 404 and 457 nm. The spectral components correspond to the discrete emitting structures in the molecules. The higher number of spectral components in the spectrum of compound **2** in comparison with the compound **7** indicates higher number of discrete emitting structures in compound **2** and consequently more complex spectrum. The components of the spectrum of compound **2** are red shifted, comparing with the components of the spectrum of compound **7**. This might be attributed to the electron-accepting competition between the pyridine ring and ester groups in compound **7**. It also should be noted that the alkyl tails in compound **7** can promote self-association of molecules, especially in polar solvents.

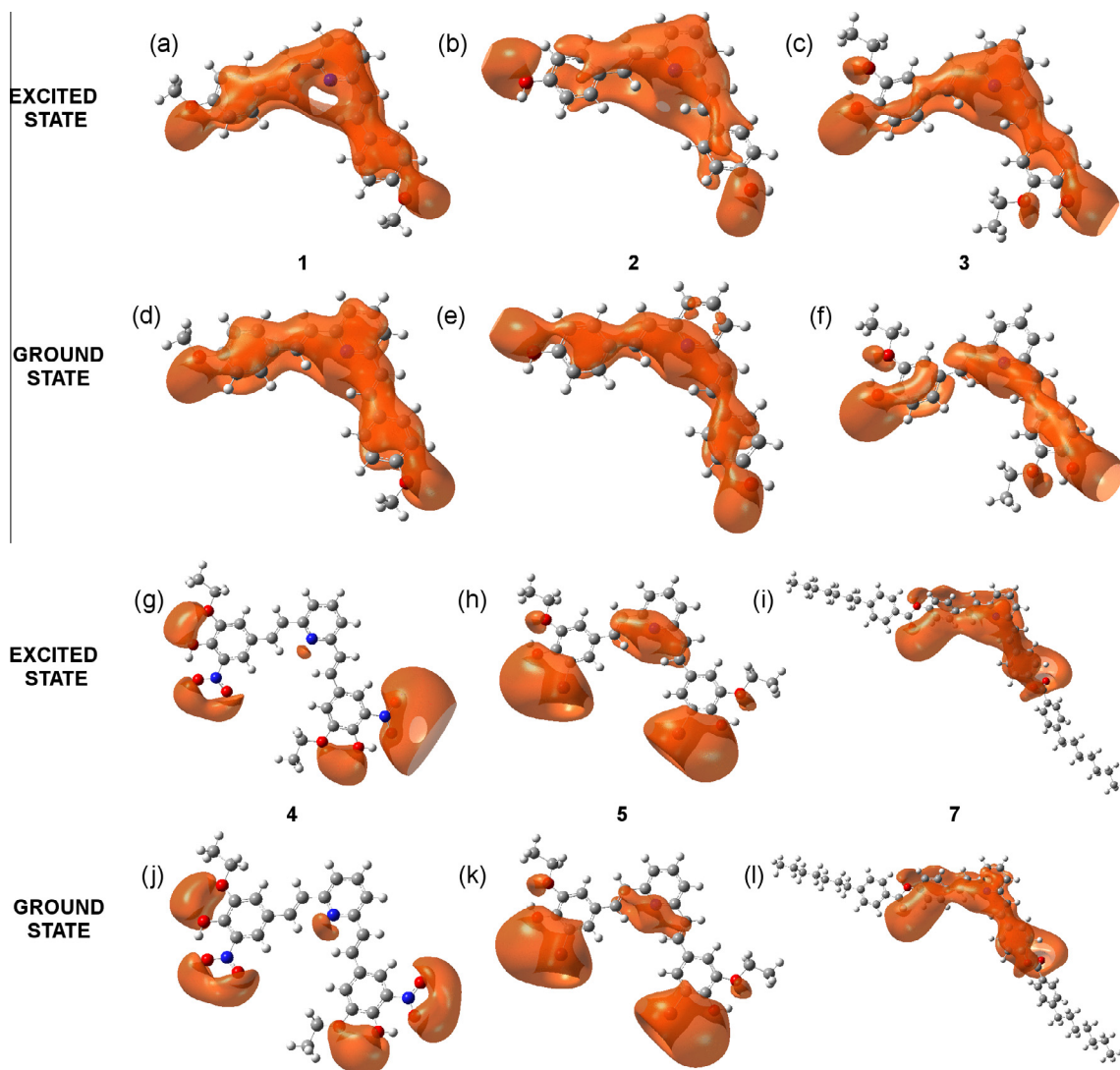


**Fig. 10.** Negative lobe of the electrostatic potential of compounds **1–5, 7** in ground and in excited states, obtained from total self-consistent field (SCF) density, or total CI density of geometries optimized on DFT level of theory, depicted on isocontour level of 0.02, or 0.03 (for compound **4**)  $e \text{ \AA}^{-2}$ .

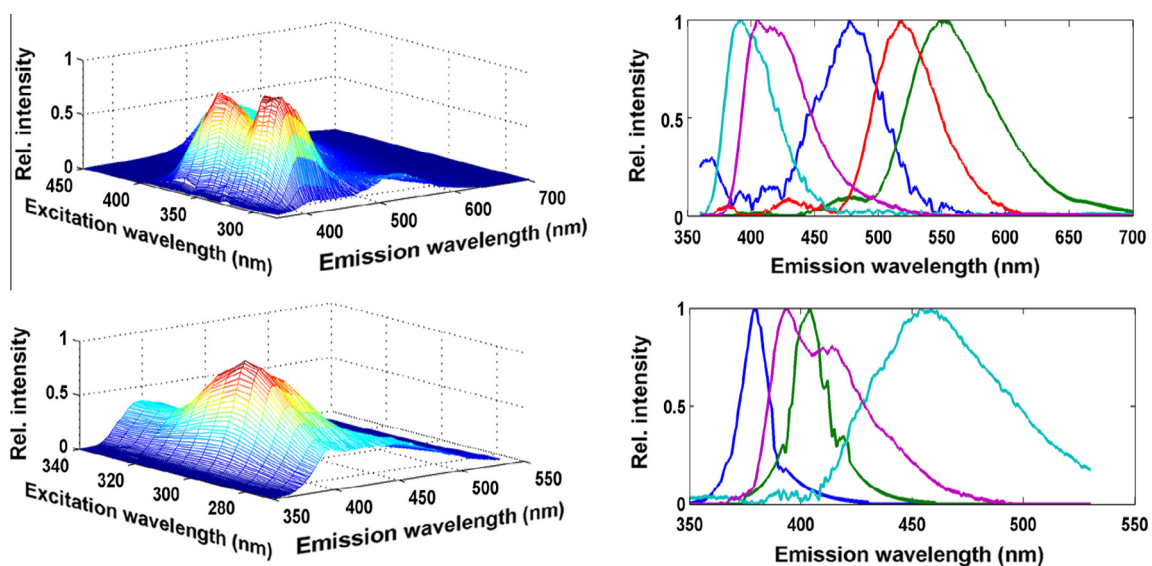


**Fig. 11.** Fluorescence landscapes (left) and corresponding spectral components (right) obtained by the MCR analysis, for the compound **2** (upper panel) and compound **7** (lower panel) in chloroform.

## Conclusion

We reported synthesis and spectral properties of symmetrical 2,6-distyrylpyridine derivatives. To the best of our knowledge, for the first time in literature the NAMFIS analysis, from NMR data and *in silico* obtained conformational assembly, was used to estimate population of conformers in solution of the representative compound from this class (compound **1**). Results of such analysis were used in attempt to explain the shape of the UV–Vis spectrum of compound, which comprise few overlapped absorption maxima. The goal is achieved with a limited success, but reveals that conformation assembly of compound is more complex than was assumed in so far published literature data, which rely on three ‘ideal’ conformers mutually different in the configuration (*s-cis* or *s-trans*) of  $\text{Py}-\text{CH}=\text{CH}-$  bonds.

Spectral and photophysical properties of the investigated compounds were studied in solvents of the different polarity and the different hydrogen bonding ability. It was found that the neutral compounds show positive solvatochromic properties, while the compound with the *N*-methylated pyridinium nitrogen exhibits a negative solvatochromism. Solvent effects on the shifts of the fluorescence maxima are more pronounced when compared with the absorption spectra. The obtained Stokes shift values (>100 nm in some cases) can be related to the strong ICT character of the investigated compounds. ICT transitions were activated to a different extent depending on the substitution pattern of the outer phenyl rings, or *N*-methylation of the central pyridine ring.

## Acknowledgements

The Ministry of Education, Science and Technological Development of the Republic of Serbia supported this work; Grants No. 172013, 172035 and 173017. The work reported makes use of results produced by the High-Performance Computing Infrastructure for South East Europe’s Research Communities (HP-SEE), a project cofunded by the European Commission (under Contract Number 261499) through the Seventh Framework Programme HP-SEE (<http://www.hpsee.eu/>). Authors gratefully acknowledge computational time provided on PARADOX cluster at the Scientific Computing Laboratory of the Institute of Physics Belgrade (SCL-IPB), supported in part by the Serbian Ministry of Education, Science and Technological Development under Projects No. ON171017 and III43007, and by the European Commission under FP7 Projects PRACE-3IP and EGI-InSPIRE.

## Appendix A. Supplementary material

Supplementary data associated with this article can be found, in the online version, at <http://dx.doi.org/10.1016/j.saa.2014.07.023>.

## References

- [1] T. Deligeorgiev, A. Vasilev, S. Kaloyanova, J.J. Vaquero, *Color. Technol.* 126 (2010) 55–80.
- [2] C.-C. Lee, A.T. Hu, *Dyes Pigm.* 59 (2003) 63–69.
- [3] C. Qin, M. Zhou, W. Zhang, X. Wang, G. Chen, *Dyes Pigm.* 77 (2008) 678–685.
- [4] S. Shettigar, G. Umesh, P. Poornesh, K.B. Manjunatha, A.M. Asiri, *Dyes Pigm.* 83 (2009) 207–210.
- [5] M. Matsui, K. Ooiwa, A. Okada, Y. Kubota, K. Funabiki, H. Sato, *Dyes Pigm.* 99 (2013) 916–923.
- [6] E. Lukovskaya, Y. Glazova, Y. Fedorov, A. Boblylova, A. Mizerev, A. Moiseeva, A. Anisimov, A. Peregodov, O. Fedorova, *Dyes Pigm.* 104 (2014) 151–159.
- [7] G. Bartocci, A. Spalletti, U. Mazzucato, in: J. Waluk (Ed.), *Conform. Anal. Mol. Excit. States*, Wiley, New York, 2000 (Chapter 5).
- [8] V.M. Chapela, M.J. Percino, C. Rodríguez-Barbarín, *J. Chem. Crystallogr.* 33 (2003) 77–83.
- [9] F.J. Melendez, O. Urzúa, M.J. Percino, V.M. Chapela, *Int. J. Quantum Chem.* 110 (2010) 838–849.
- [10] L. Giglio, U. Mazzucato, G. Musumarra, A. Spalletti, *Phys. Chem. Chem. Phys.* 2 (2000) 4005–4012.
- [11] H. Wang, R. Helgeson, B. Ma, F. Wudl, *J. Org. Chem.* 65 (2000) 5862–5867.
- [12] X. Xu, W. Qiu, Q. Zhou, J. Tang, F. Yang, Z. Sun, P. Audebert, *J. Phys. Chem. B* 112 (2008) 4913–4917.
- [13] P.P. Madeira, C.A. Reis, A.E. Rodrigues, L.M. Mikheeva, B.Y. Zaslavsky, *J. Phys. Chem. B* 114 (2010) 457–462.
- [14] I. Shehata, *Helv. Chim. Acta* 85 (2002) 2125–2137.
- [15] P. Vallat, W. Fan, N. El Tayar, P.-A. Carrupt, B. Testa, *J. Liq. Chromatogr.* 15 (1992) 2133–2151.
- [16] M.J. Kamlet, J.-L.M. Abboud, M.H. Abraham, R.W. Taft, *J. Org. Chem.* 48 (1983) 2877–2887.
- [17] J. Catalán, *J. Phys. Chem. B* 113 (2009) 5951–5960.
- [18] A. Marini, A. Muñoz-Losa, A. Biancardi, B. Mennucci, *J. Phys. Chem. B* 114 (2010) 17128–17135.
- [19] J. Marković, N. Trišović, T. Tóth-Katona, M. Milčić, A. Marinković, C. Zhang, A.J. Jákli, K. Fodor-Csorba, *New J. Chem.* 38 (2014) 1751–1760.
- [20] E.D. Bergmann, S. Pinchas, *J. Org. Chem.* 15 (1950) 1184–1190.
- [21] J. Mendieta, M.S. Diaz-Cruz, M. Esteban, R. Tauler, *Biophys. J.* 74 (1998) 2876–2888.
- [22] R.W. Harrison, *J. Comput. Chem.* 14 (1993) 1112–1122.
- [23] A. Pedretti, L. Villa, G. Vistoli, *J. Comput. Aided Mol. Des.* 18 (2004) 167–173. <<http://www.ddl.unimi.it>>.
- [24] D.A. Evans, M.J. Bodkin, S.R. Baker, G.J. Sharman, *Magn. Reson. Chem.* 45 (2007) 595–600.
- [25] O. Atasoylu, G. Furst, C. Risatti, A.B. Smith III, *Org. Lett.* 12 (2010) 1788–1791.
- [26] J.J.P. Stewart, MOPAC2012, Stewart Computational Chemistry, Colorado Springs, CO, USA. <<http://openmopac.net>>.
- [27] J.J.P. Stewart, *J. Mol. Model.* 13 (2007) 1173–1213.
- [28] M.J. Frisch, G.W. Trucks, H.B. Schlegel, G.E. Scuseria, M.A. Robb, J.R. Cheeseman, J.A. Montgomery Jr., T. Vreven, K.N. Kudin, J.C. Burant, J.M. Millam, S.S. Iyengar, J. Tomasi, V. Barone, B. Mennucci, M. Cossi, G. Scalmani, N. Rega, G.A. Petersson, H. Nakatsuji, M. Hada, M. Ehara, K. Toyota, R. Fukuda, J. Hasegawa, M. Ishida, T. Nakajima, Y. Honda, O. Kitao, H. Nakai, M. Klene, X. Li, J.E. Knox, H.P. Hratchian, J.B. Cross, V. Bakken, C. Adamo, J. Jaramillo, R. Gomperts, R.E. Stratmann, O. Yazyev, A.J. Austin, R. Cammi, C. Pomelli, J.W. Ochterski, P.Y. Ayala, K. Morokuma, G.A. Voth, P. Salvador, J.J. Dannenberg, V.G. Zakrzewski, S. Dapprich, A.D. Daniels, M.C. Strain, O. Farkas, D.K. Malick, A.D. Rabuck, K. Raghavachari, J.B. Foresman, J.V. Ortiz, Q. Cui, A.G. Baboul, S. Clifford, J. Cioslowski, B.B. Stefanov, G. Liu, A. Liashenko, P. Piskorz, I. Komaromi, R.L. Martin, D.J. Fox, T. Keith, M.A. Al-Laham, C.Y. Peng, A. Nanayakkara, M. Challacombe, P.M.W. Gill, B. Johnson, W. Chen, M.W. Wong, C. Gonzalez, J.A. Pople, *Gaussian03/09*, Revision C.02 2003/2009.
- [29] Jmol: an open-source Java viewer for chemical structures in 3D. <<http://www.jmol.org/>>.
- [30] J.E. Ridley, M.C. Zerner, *Theor. Chem. Acc.* 32 (1973) 111–134.
- [31] G. Cruciani (Ed.), *Molecular Interaction Fields. Applications in Drug Discovery and ADME Prediction*, Wiley-VCH, Zürich, Switzerland, 2006.
- [32] GRID Version 22c, Molecular Discovery Ltd. <<http://www.moldiscovery.com>>.
- [33] P.J. Goodford, *J. Med. Chem.* 28 (1985) 849–857.
- [34] P. Jacques, B. Graff, V. Diemer, E. Ay, H. Chaumeil, C. Carré, J.-P. Malval, *Chem. Phys. Lett.* 531 (2012) 242–246.
- [35] H. Xiao, C. Mei, N. Ding, T. Wei, Y. Zhang, B. Li, *J. Photochem. Photobiol., A: Chem.* 273 (2014) 29–33.
- [36] J.R. Lakowicz, *Principles of Fluorescence Spectroscopy*, Springer, Singapore, 2006.
- [37] U. Mazzucato, F. Momicchioli, *Chem. Rev.* 91 (1991) 1679–1719.
- [38] D.O. Cicero, G. Barbato, R. Bazzo, *J. Am. Chem. Soc.* 117 (1995) 1027–1033.
- [39] C.D. Blundell, M.J. Packer, A. Almond, *Bioorg. Med. Chem.* 21 (2013) 4976–4987.
- [40] I. Kikaš, B. Carlotti, I. Škorić, M. Šindler-Kulyk, U. Mazzucato, A. Spalletti, *J. Photochem. Photobiol., A: Chem.* 244 (2012) 38–46.
- [41] T. Clark, M. Hennemann, J.S. Murray, P. Politzer, *J. Mol. Model.* 13 (2007) 291–296.